Effect of Catalyst Pre-Treatment on Chirality-Selective Growth of Single-Walled Carbon Nanotubes

Martin Fouquet,[1,#] Bernhard C. Bayer,[1,#,*] Santiago Esconjauregui,[1]
Christian Thomsen,[2] Stephan Hofmann,[1] John Robertson[1]

[1]*Department of Engineering, University of Cambridge, Cambridge CB3 0FA, United Kingdom*
[2]*Institut für Festkörperphysik, Technische Universität Berlin, 10623 Berlin, Germany*

Abstract

We show that catalyst pre-treatment conditions can have a profound effect on the chiral distribution in single-walled carbon nanotubes chemical vapor deposition. Using a SiO_2-supported Cobalt model catalyst and pre-treatment in NH_3, we obtain a comparably narrowed chiral distribution with a downshifted tube diameter range, independent of the hydrocarbon source. Our findings demonstrate that the state of the catalyst at the point of nanotube nucleation is of fundamental importance for chiral control, thus identifying the pre-treatment atmosphere as a key parameter for control of diameter and chirality distributions.

Keywords:
Single-walled Carbon Nanotubes; Chirality; Chemical Vapor Deposition; Pre-Treatment; Ammonia; Cobalt Catalyst

[#] Equally contributed

[*] Corresponding Author: Tel.: +44/(0)1223/748291, Fax: +44/(0)1223/748348, Email: bcb25@cam.ac.uk

1. Introduction

It is well known in heterogeneous catalysis[1] in general and in catalytic chemical vapor deposition (CVD) of carbon nanotubes[2,3] in particular that catalyst pre-treatment conditions can strongly affect the properties of the products of the catalyzed reactions. Here, we use a model catalyst system for growth of single-walled carbon nanotubes (SWNTs) to study such an influence of catalyst pre-treatment on the chiral distribution of the grown SWNTs.

The remarkable thermal, mechanical and electronic properties of single-walled carbon nanotubes are specifically related to their structure, which is uniquely described by their individual chiral index (n, m).[4] Controlling structural selectivity during the synthesis would thus be beneficial for many of the potential applications of SWNTs. A large range of recent reports concentrated on growth of SWNTs with a narrow (n, m) distribution by CVD, as this synthesis method is the most versatile and promising technique not only in terms of bulk production but also for device integration.[5–9]

It has previously been suggested that, after an initial pre-treatment step before hydrocarbon exposure that determines the distribution of catalyst particle sizes/faceting/reconstructions, two factors control the chiral distribution in CVD (Figure 1). First, at the point of SWNT nucleation, the relationship between the size/faceting/reconstruction of a given catalyst nanoparticle and a given nanotube cap leads to nucleation of a particular (n, m) cap.[10–12] Secondly, during continued growth of the nanotubes, the growth rate for an already nucleated nanotube can vary with its chiral index.[13–15] This will in turn modify the material fraction of nanotube material with a particular (n, m) in a bulk SWNT sample. Thus, the eventual chiral distribution of the nanotube material after CVD, as measured by techniques like Raman spectroscopy, is the result of both factors, where it is still under debate which factor is governing.

Chiral selectivity in CVD has previously been achieved by very specific multi-component catalyst and/or support designs, including bimetallic catalysts[16–22] or mesoporous supports.[23–31] Alternatively, for a given catalyst/support combination, empirically optimized temperature profiles[26,32–35] or specific growth[36–40] or pre-treatment atmospheres[12] have resulted in narrowing of the dispersion of (n, m) indices. For instance, engineering of the pre-treatment gas mixture ($Ar/He/H_2/H_2O$) has been shown to result in an increased fraction of metallic SWNTs[12]. It has also been reported that the type of carbon precursor during CVD has an impact on the resulting SWNT chiral distribution.[17,37,41,42] Likewise, the addition of small amounts of ammonia (NH_3) during growth was recently shown to change the chiral distribution towards large diameter (n, m)[43] for SWNT growth and to induce an "epitaxial" growth mode for multi-walled nanotubes.[44,45] However, the actual mechanisms behind the beneficial effects of the various add-elements and gaseous

species, and whether these act during nucleation or growth or during both stages, remain largely elusive. This incomplete understanding is mainly caused by the tremendous complexity of the multidimensional parameter space of catalyst components, support properties, pre-treatment and growth gas mixtures and temperature profiles, where each of these factors could potentially change (n, m) distributions.

Here, to isolate the effect of the catalyst pre-treatment, we use a simple monometallic Co catalyst on SiO_2 wafer support and expose this model catalyst to a two-step CVD process (Figure 2a). First, we pre-treat in pure NH_3 or, for reference, vacuum or Argon (Ar), which is then followed by exposure to an undiluted hydrocarbon species (C_2H_2 or Ethanol vapor). Multi-wavelength Raman spectroscopy on the as-grown SWNTs reveals that for both hydrocarbon precursor gases the pre-treatment in NH_3 consistently narrows the obtained diameter range and chiral distribution towards smaller diameter SWNTs. This suggests that the state of the catalyst particle before hydrocarbon exposure and nanotube nucleation is of key importance for the resulting chirality distribution. Thus, optimization of the pre-treatment atmosphere is shown to be a crucial parameter to control chiral selectivity in CVD.

2. Experimental Details

We prepare the model catalyst by thermal evaporation of a Cobalt film, nominally 0.1 nm thick, onto silica (SiO_2, 200 nm) coated Si wafers. Nominal thickness is measured by an in-situ quartz crystal microbalance. Note that the Co film is oxidized during subsequent sample transfer/storage in ambient air.[32] A custom-built low pressure chemical vapor deposition system is employed for CVD (base pressure 10^{-6} mbar). See Figure 2a for a schematic sketch of the process: Firstly, the Co catalyst film is annealed at 700 ºC in undiluted NH_3 (10^{-3} mbar for C_2H_2 growth and 5 mbar for Ethanol growth, ramp up in gas 1 min, hold time at temperature 4 min). The NH_3 pre-treatment is compared to pre-treatment anneals in vacuum (10^{-6} mbar, ramp up in vacuum 1 min, hold time at temperature 4 min) or undiluted Ar (10^{-3} mbar for C_2H_2 growth, ramp up in Ar 1 min, hold time at temperature 4 min). Secondly, the pre-treatment is directly followed (after short pump to vacuum, gas exchange time < 30s) by nanotube growth at 700 ºC in either undiluted acetylene (C_2H_2, 10^{-3} mbar controlled via mass-flow controller) or undiluted Ethanol vapor (CH_3CH_2OH, 5 mbar, provided via leak valve from liquid Ethanol reservoir at room temperature). Growth time is 15 min, after which the hydrocarbon gas is pumped out and the sample is left to cool in vacuum to room temperature (~20 min). Note that great care was taken to exclude gas atmosphere related cooling effects by cross-checking the sample temperature with a combination of pyrometric and thermocouple measurements and adjustment of the electric current through the resistive sample heater to obtain a constant temperature across the various treatments.

The resulting nanotube morphology is characterized by scanning electron microscopy (SEM, FEI XL30). The morphology of samples that only underwent pre-treatment (i.e. no hydrocarbon exposure) is characterized using atomic force microscopy (AFM, Veeco Dimension in non-contact mode).

Structural assignments of the SWNTs are done by multi-wavelength Raman spectroscopy for eight different excitation energies from 1.96 - 2.66 eV. We employ two Raman systems; a confocal triple monochromator setup (Dilor XY800) for 2.18 and 2.41 - 2.66 eV, and a Labram (HR800, Horiba Jobin Yvon) for 1.96 and 2.33 eV. The monochromated Dilor setup does not employ a notch-filter allowing to measure down to low wavenumbers, while the Labram setup has a notch-filter cut-off at ~180 cm^{-1} for 1.96 eV and at ~140 cm^{-1} for 2.33 eV. All Raman measurements are in backscattering geometry and recorded with a charge coupled device on as-prepared SWNTs samples. We convert radial breathing mode (RBM) peaks in the Raman spectra to diameters.[46] Assignment to chiral indices (n, m) is done by including the obtained diameters together with the excitation energies E_{laser} in a theoretical Kataura plot.[47,48] The abundance $A_{(n, m)}$ of an individual (n, m) is estimated by:[32]

$$A_{(n,m)} \propto \frac{I_{\exp}(RBM)}{I_{Si} \times I_{theo}(n,m)} \qquad \text{(Eqn. 1)}$$

with the RBM intensity $I_{exp}(RBM)$, the Si peak Raman intensity I_{Si} and the maximum Raman intensity $I_{theo}(n, m)$ by theory.[48] See ref. [32] for details and limitations of the methods used for assignment and abundance estimation. We note that we cross-checked Raman signatures across several spots for each sample for selected wavelengths and also confirmed for selected growth conditions and selected wavelengths that RBM signatures are reproducible for repeated CVD runs, indicating that our measurements indeed capture generic chiral distributions for the growth conditions used. We also note that we have previously confirmed that nanotube diameters derived by our RBM analysis method are in good agreement with high-resolution transmission electron microscopy derived diameters.[32]

As a general comment, we note that chiral abundance estimations have to always be considered with respect to the method with which they were measured. Integral characterization techniques such as Raman spectroscopy (as used here), optical absorption spectroscopy and photoluminescence excitation spectroscopy[17,29–32,42] probe the material fraction of chiral distribution in a given bulk SWNT sample. This implies that these integral techniques do not probe the number fraction of SWNTs with a given (n, m), unless all probed tubes are of roughly the same length. In contrast, point-localized probes such as electron diffraction[39,41,43,49] probe individual tubes and thus statistics from such point probe techniques commonly provide number fractions of SWNTs with a particular (n, m), unless the length of tubes is considered.

3. Results

For all NH_3 and vacuum pre-treatments nanotubes are grown in entangled form and homogeneously cover the entire wafer surface (SEM micrographs in Figure 2b). A semi-quantitative estimation of nanotube yield based on Raman intensities (ratios of nanotube G-peak and Si-substrate-peak intensities I(G)/I(Si) quoted in Figure 2b) shows that for both C_2H_2 and Ethanol growth the vacuum pre-treatment results in a thicker film/higher coverage of entangled nanotubes compared to NH_3 pre-treatment i.e. vacuum pre-treatment results in increased nanotube yield. Comparing the hydrocarbon sources, Ethanol consistently gives a somewhat higher yield than C_2H_2. In contrast, pre-treatment in Ar resulted in a much lower yield of only sparse nanotubes.

The result of the chiral assignment for the C_2H_2-based growth is summarized in Figure 3 comparing pre-treatment in NH_3 (Figure 3a) and vacuum (Figure 3c). The multi-wavelength Raman spectra, which are used for the assignments, are shown alongside the chiral maps for both pre-treatment conditions in Figure 3b and Figure 3d, respectively. For each pre-treatment condition 34 (n, m) are assigned, but the diameter range for NH_3 pre-treatment based on the (n, m) is 0.68 - 1.39 nm, whereas the diameter range for tubes grown after vacuum pre-treatment is larger with 0.63 - 1.49 nm (note that the data for vacuum pre-treated growth by C_2H_2 is taken from ref. [32]). We note that for C_2H_2 growth substitution of the NH_3 pre-treatment with inert Ar pre-treatment at the same total pressure resulted in a strongly reduced growth of nanotubes (which we attribute to incomplete formation of active catalyst nanoparticles, see below), impeding chiral assignments for these conditions.

Assigned (n, m) alongside the multi-wavelength Raman spectra for Ethanol-based growth are shown in Figure 4 for the pre-treatment in NH_3 (Figure 4a,b) compared to vacuum pre-treatment (Figure 4c,d). Here, the NH_3 pre-treatment results in 39 (n, m) with a diameter range of 0.64 - 1.56 nm. In contrast, the vacuum pre-treatment yields an assignment of 47 different (n, m) in a diameter range of 0.75 - 1.87 nm. We note that for vacuum pre-treated growth by Ethanol the large diameter tubes (≥1.7 nm) are extremely difficult to assign because of a strongly increasing number of assignment possibilities.[32] However, the Raman intensity for tubes in this range is rather low and thus the influence on the overall abundance of the (n, m) ensemble is small.

The estimated abundance is shown by the column height (Figure 3a,c and Figure 4a,c), with (n, m) of abundance ≤1% shown in faded blue. Additionally the abundance is plotted as function of the SWNT diameter in Figure 5. Note that the raw data of the chiral maps is tabulated in the Supporting Information.

For the C_2H_2-based growth with NH_3 pre-treatment the most abundant tubes are the (6,5) (34.5%), (7,5) (14.8%) and (9,2) (8.4%). About 82% of all tubes are semiconducting and 76% of all

tubes are in the very narrow diameter interval of 0.75 - 0.90 nm, and we note that only 5 chiralities can account for 68% of all tubes. This compares to a wider chiral distribution for C_2H_2 growth after vacuum pretreatment, where the most abundant tubes are the (7,5) (14.3%), (7,6) (11.4%) and (10,9) (10.5%). The diameter interval in which about 76% of all tubes are found, is larger with 0.75 - 1.28 nm. The amount of semiconducting tubes is slightly reduced to 76% and only about half of all tubes (53%) are made up by the five most abundant (n, m). Thus for C_2H_2 growth the NH_3 pre-treatment results in a narrowing of both the chiral distribution and of the SWNT diameter range towards smaller diameters.

The SWNTs grown by Ethanol show a similar behavior. For growth after pre-treatment by NH_3 the most abundant chiral indices are (7,6) (11.2%), (7,7) (10.5%) and (10,9) (7.7%). The majority (75%) of all tubes are in the diameter interval of 0.75 - 1.26 nm and 74% are semiconducting. The pre-treatment in vacuum prior to Ethanol growth results in a wider chiral distribution and the most abundant chiral indices are (14,9) (12.5%), (9,8) (10.0%) and (10,9) (8.9%). About 77% of all tubes are in the diameter range of 1.15 - 1.87 nm and 78% are semiconducting. As above for C_2H_2, the NH_3 pre-treatment narrows and downshifts diameter and chiral range also for Ethanol growth.

We note that the overall tube diameter range for Ethanol growth is larger than for C_2H_2 growth despite having similar pre-treatment conditions. Generally, highly abundant tubes are mainly found at large chiral angles, which is in good agreement with literature for both experiment[16–21,25,27,34,39] and theory.[11,13,15] This may be related to higher growth rates.[14]

It has previously been reported that catalyst particle size distributions can change as a function of temperature[26,32] (constant in this study) as well as pre-treatment atmosphere.[50,51] Such pre-treatment atmosphere dependent differences in catalyst particle size distributions may in turn determine the resulting nanotube diameters. Therefore, we compare catalyst particle sizes for our pre-treatment conditions. In Figure 6 we study samples that only underwent pre-treatment (i.e. no hydrocarbon exposure) in NH_3 or vacuum. Our AFM analysis shows that under our processing conditions both NH_3 and vacuum pre-treatments give similar distributions of nanoparticle sizes. This suggests that under our low pressure pre-treatment conditions the particle size distribution is mainly determined by the annealing temperature. This may be related to interfacical stabilistation of Co nanoparticles on SiO_2, as we have previously shown by in-situ X-ray photoelectron spectroscopy.[32]

4. Discussion

Figure 1 had summarized the current model for chiral selectivity selection during CVD: First, the selective nucleation of (n, m) nanotube caps results from a relationship between a given nanotube cap and the size/faceting/reconstruction of a given catalyst nanoparticle at the point of nanotube nucleation.[11,12] The size/faceting/reconstruction distribution of a catalyst nanoparticle ensemble is in turn determined by the pre-treatment conditions. During further growth of the nanotube, the chiral index (n, m) of the initially nucleated cap is then kept because of the high energy cost for a change of chirality of an entire nanotube. Therefore, the initial number fraction of an individual (n, m) in a nanotube ensemble is determined at the point of nucleation. Secondly, however, the growth rates of already nucleated nanotubes can vary with their chiral indices. These inhomogeneous growth rates may either be caused by easier addition of carbon atoms to some (n, m)-tubes[13–15] or by etching effects induced by the process conditions.[43] Growth-rate effects will influence the material fraction of nanotube material with a given (n, m) within a SWNT bulk sample. Thus, the resulting overall abundance (material fraction of nanotube material) of a given chiral index (n, m) in a nanotube ensemble results from (n, m)-selective effects during both nucleation and growth. It is still under debate whether nucleation or growth-rate effects are governing obtainable nanotube chiral distributions. We now discuss our observations in light of this question.

Most importantly, our observation that for constant hydrocarbon exposure conditions the diameter range and chiral distribution can be narrowed and downshifted by simply changing the pre-treatment condition (NH_3 versus vacuum) strongly supports the idea that the state of the catalyst at the point of nucleation selects the initial chiral distribution. Thus optimization of the pre-treatment environment is one of the key parameters in CVD to selectively grow nanotubes of particular chiral indices.

We emphasize that in our experiments the NH_3 is used only to pre-condition the catalyst before the carbon source is introduced into the CVD system. Therefore, the NH_3 atmosphere acts on the state of the catalyst nanoparticles *before* the initial nanotube cap is formed. Our AFM analysis of only pre-treated samples (Figure 6) indicates no substantial differences in catalyst particle sizes from the different pre-treatments (NH_3 vs vacuum). This implies that under our low-pressure pre-treatment conditions not catalyst nanoparticle size differences but rather additional effects from the pre-treatment conditions such as faceting/reconstructions determine the resulting chiral distribution. When we compared NH_3 pre-treatment with inert Argon pre-treatment at the same total pressure we found a strongly decreased nanotube growth from the Ar pre-treatment. This excludes that the total pressure difference between vacuum and NH_3 pre-treatments is the reason for the change in

chirality, and rather implies a chemical interplay of the NH_3 with the catalyst. Exposure of transition metal catalysts to nitrogen compounds can alter their subsequent carbon uptake characteristics during hydrocarbon exposure.[44] Cobalt is a known catalyst for decomposition of NH_3.[52,53] At our CVD temperatures NH_3 is know to dissociatively adsorb onto Co,[54] thus reducing the Co-oxide that is initially present due to ambient air exposure of our films. We note however that we have previously shown that also the vacuum pre-treatment alone leads to full Co-oxide reduction.[32] Exposing Co(-oxides) to atmospheric pressure NH_3 at 700 ºC was reported to lead to formation of (metastable) bulk Co nitride nanoparticles[55] while for smaller NH_3 pressures changes in the faceting of metallic Co nanoclusters[56] as well as changes in surface reconstructions of similar transition metal catalysts[1,57] have been reported. We have previously studied the evolution of Co catalyst films (similar to the ones used in the present study) during thermal pre-treatments in NH_3 for multi-walled nanotube growth.[58] There we found from X-ray photoelectron spectroscopy no evidence of bulk Co-nitride formation under similar NH_3 pressures as used in the present study. This suggests that for the present conditions the NH_3 treatment results in the adoption of different faceting/surface reconstruction distributions of the Co nanoparticles (as compared to vacuum). The differences in faceting/surface reconstruction distributions between pre-treatments then result in different distributions of chiral caps formed when the hydrocarbon is introduced (see Table of Contents Figure for a schematic illustration). In this context, it has also been recently suggested based on theoretical calculations that nitrogen-adsorption on Co catalysts can modify the binding energy between the nanoparticles and growing nanotube nuclei, thus modifying the resulting nanotube structure.[59] While possible chirality dependent effects on growth rate[13–15] or etching effects[43] may also play a role during the continued CVD our data clearly shows that the chirality distribution can be selected by the processing prior hydrocarbon exposure i.e. by the pre-treatment.

Our findings are consistent with previous reports concerning the differences between Ar/He/H_2/H_2O pre-treatments,[12] where changes in the pre-treatment atmosphere composition led to changes in the SWNT chiral distribution. For the particular effect of nitrogen species, we note that our observed shift to smaller diameters from nitrogen-containing pre-treatment is consistent with recent work[37,38] on acetonitrile addition *during* CVD that resulted in a downshift of SWNT diameters but different to another previous report[43] where NH_3 addition *during* growth was found to lead to larger SWNT tube diameters (as compared to NH_3-free reference growth conditions). This implies that the presence of the same element/gas at different points in different CVD recipes with different catalyst/support combinations can have drastically different effects.

While both C_2H_2 and Ethanol both consistently showed downshifted and narrower chiral distributions after NH_3 pre-treatment, both precursors still showed different overall yield and chiral distributions. This is in line with previous literature.[17,39,41,42] Several suggestions have previously

been made to explain (n, m) dependence on carbon source: For instance, selective cap formation from particular intermediate carbon species provided by a particular precursor onto a particularly facetted catalyst nanoparticle has been suggested[41] and theoretical calculations have shown that different intermediate carbon species (from different precursor gases) can influence resulting chirality.[60] Alternatively, the carbon supply rate as a function of the precursor-dependent chemical potential/dissociation rate was suggested to select different nanotube diameters from a constant set of nanoparticles.[61] Finally, also reactions with precursor decomposition by-products, such as hydrogen[17] or oxygen-containing precursor fragments (e.g. –OH groups from Ethanol[62,63]), may change yield, chirality and diameter distributions between different carbon precursors.

We have previously obtained a similarly narrow diameter distribution for C_2H_2 even without the use of NH_3 from the same Co catalyst by lowering of the growth temperature to 600 ºC while using only vacuum pre-treatment.[32] However, comparing the (n, m) distribution between these two similarly narrow diameter distributions, we find that vacuum/600 ºC leads to a majority (55%) of metallic tubes,[32] while NH_3/700 ºC shows a majority (82%) of semiconducting tubes for C_2H_2 growth. This implies that diameter evolution and (n, m) evolution can be independently controlled by engineering of growth temperature and pre-treatment atmosphere as individual parameters.

Finally we want to comment on the limitations of our study: The model in Figure 1 is certainly a simplification of the real situation during chiral selective nanotube growth. First, nucleation and growth are not as separated steps as implied by the model but are actually two interconnected aspects of one single process. Second, catalyst nanoparticles were previously shown to not remain static during hydrocarbon exposure and nanotube nucleation but rather to deform throughout nanotube growth.[64] This implies that catalyst-support interactions will also have an impact on chirality selective SWNT growth, in particular since Co nanoparticles can be interfacially stabilised on SiO_2.[32] Third, catalyst nanoparticles may also change their faceting/surface reconstructions during the initial moments of hydrocarbon exposure (i.e. after pre-treatment but before nanotube nucleation occurs) due to adsorption of carbon precursor fragments.[65] As a fourth and general point we note that a given pre-treatment (such as NH_3) which changes the faceting/reconstruction of catalyst particles could change chiral distributions by various mechanisms: (a) A given catalyst particle, that is also active without pre-treatment, could nucleate a different chirality SWNT due to different faceting from the pre-treatment (leaving the overall catalytic activity unaffected, see Table of Contents Figure for a schematic illustration of this possible mechanism). (b) A nanoparticle that is inactive without the pre-treatment could nucleate a certain (additional) (n, m) when pre-treated (increasing overall catalytic activity). (c) A nanoparticle that nucleates a certain chirality without pre-treat could be deactivated by the pre-treatment, thus removing that certain chirality via pre-treatment (and reducing overall catalytic activity).

Coexistence of all three mechanisms (a-c) is conceivable for a catalyst particle distribution. In our data, the reduced nanotube yield from NH_3 pre-treatments compared to vacuum pre-treatments for both C_2H_2 and Ethanol (Figure 2b) could indicate a (partial) catalyst deactivation process (as in (c)). However, the additional occurrence (for both C_2H_2 and Ethanol) of chiral indices in our NH_3 pre-treatment samples that are not present in the vacuum pre-treatment samples (Figures 3 and 4) excludes that catalyst deactivation is the only mechanism under our conditions and rather implies also catalyst activation (as in (b)) or changes in nucleating catalyst-nanotube cap combinations (as in (a)) from the NH_3 pre-treatment. To conclusively answer which mechanism(s) are occurring point-localised information relating Co nanoparticle faceting and SWNT chirality for a statistically relevant number of nucleations would be required, which is beyond the scope of this study. Nevertheless, our observation that changes in catalyst pre-treatment can change the chiral distributions for constant growth conditions underscores the importance of catalyst pre-treatment in chirality-selective SWNT growth.

Conclusions

In summary we have shown that the chiral and diameter distribution for CVD grown SWNTs can be narrowed towards smaller diameters solely based on the pre-treatment conditions (here for NH_3), independent of the growth conditions and carbon precursor. This emphasizes that the state of the catalyst at the point of nanotube nucleation is of key importance for future strategies towards chiral control in single-walled nanotube growth.

Acknowledgements

We acknowledge XXX for funding. B.C.B acknowledges a Research Fellowship at Hughes Hall, Cambridge. J.R. thanks the Alexander von Humboldt Foundation for support.

Supporting Information Available

Discussion of particle height/nanotube diameter relationships for Figures 5 and 6. Raw data of chiral abundance analysis.This information is available free of charge via the Internet at http://pubs.acs.org.

References

(1) Strongin, D. R.; Somorjai, G. A. Ammonia-Pretreatment-Induced Restructuring of Iron Single-Crystal Surfaces: Its Effects on Ammonia Synthesis and on Coadsorbed Aluminum Oxide and Potassium. *J. Catal.* **1989**, *118*, 99–110.

(2) Nessim, G. D.; Hart, A. J.; Kim, J. S.; Acquaviva, D.; Oh, J.; Morgan, C. D.; Seita, M.; Leib, J. S.; Thompson, C. V. Tuning of Vertically-Aligned Carbon Nanotube Diameter and Areal Density through Catalyst Pre-Treatment. *Nano Lett.* **2008**, *8*, 3587–3593.

(3) Esconjauregui, S.; Bayer, B.; Fouquet, M.; Wirth, C.; Yan, F.; Xie, R.; Ducati, C.; Baehtz, C.; Castellarin-Cudia, C.; Bhardwaj, S. Use of Plasma Treatment to Grow Carbon Nanotube Forests on TiN Substrate. *J. Appl. Phys.* **2011**, *109*, 114312.

(4) Reich, S.; Thomsen, C.; Maultzsch, J. *Carbon Nanotubes*; John Wiley & Sons, 2008.

(5) Robertson, J.; Zhong, G.; Esconjauregui, C. S.; Bayer, B. C.; Zhang, C.; Fouquet, M.; Hofmann, S. Applications of Carbon Nanotubes Grown by Chemical Vapor Deposition. *Jpn. J. Appl. Phys.* **2012**, *51*, 01AH01.

(6) Esconjauregui, S.; Fouquet, M.; Bayer, B. C.; Ducati, C.; Smajda, R.; Hofmann, S.; Robertson, J. Growth of Ultrahigh Density Vertically Aligned Carbon Nanotube Forests for Interconnects. *ACS Nano* **2010**, *4*, 7431–7436.

(7) Bayer, B.; Zhang, C.; Blume, R.; Yan, F.; Fouquet, M.; Wirth, C.; Weatherup, R.; Lin, L.; Baehtz, C.; Oliver, R. In-Situ Study of Growth of Carbon Nanotube Forests on Conductive CoSi2 Support. *J. Appl. Phys.* **2011**, *109*, 114314.

(8) Bayer, B.; Sanjabi, S.; Baehtz, C.; Wirth, C.; Esconjauregui, S.; Weatherup, R.; Barber, Z.; Hofmann, S.; Robertson, J. Carbon Nanotube Forest Growth on NiTi Shape Memory Alloy Thin Films for Thermal Actuation. *Thin Solid Films* **2011**.

(9) Zhang, C.; Yan, F.; Bayer, B. C.; Blume, R.; van der Veen, M. H.; Xie, R.; Zhong, G.; Chen, B.; Knop-Gericke, A.; Schlogl, R. Complementary Metal-Oxide-Semiconductor-Compatible and Self-Aligned Catalyst Formation for Carbon Nanotube Synthesis and Interconnect Fabrication. *J. Appl. Phys.* **2012**, *111*, 064310–064310.

(10) Zhu, H.; Suenaga, K.; Hashimoto, A.; Urita, K.; Hata, K.; Iijima, S. Atomic -Resolution Imaging of the Nucleation Points of Single *Small* **2005**, *1*, 1180–1183.

(11) Reich, S.; Li, L.; Robertson, J. Control the Chirality of Carbon Nanotubes by Epitaxial Growth. *Chem. Phys. Lett.* **2006**, *421*, 469–472.

(12) Harutyunyan, A. R.; Chen, G.; Paronyan, T. M.; Pigos, E. M.; Kuznetsov, O. A.; Hewaparakrama, K.; Kim, S. M.; Zakharov, D.; Stach, E. A.; Sumanasekera, G. U. Preferential Growth of Single-Walled Carbon Nanotubes with Metallic Conductivity. *Science* **2009**, *326*, 116–120.

(13) Ding, F.; Harutyunyan, A. R.; Yakobson, B. I. Dislocation Theory of Chirality-Controlled Nanotube Growth. *Proc. Natl. Acad. Sci.* **2009**, *106*, 2506–2509.

(14) Rao, R.; Liptak, D.; Cherukuri, T.; Yakobson, B. I.; Maruyama, B. In Situ Evidence for Chirality-Dependent Growth Rates of Individual Carbon Nanotubes. *Nat. Mater.* **2012**, *11*, 213–216.

(15) Dumlich, H.; Reich, S. Chirality-Dependent Growth Rate of Carbon Nanotubes: A Theoretical Study. *Phys. Rev. B* **2010**, *82*, 085421.

(16) Bachilo, S. M.; Balzano, L.; Herrera, J. E.; Pompeo, F.; Resasco, D. E.; Weisman, R. B. Narrow (n, M)-Distribution of Single-Walled Carbon Nanotubes Grown Using a Solid Supported Catalyst. *J. Am. Chem. Soc.* **2003**, *125*, 11186–11187.

(17) Lolli, G.; Zhang, L.; Balzano, L.; Sakulchaicharoen, N.; Tan, Y.; Resasco, D. E. Tailoring (n, M) Structure of Single-Walled Carbon Nanotubes by Modifying Reaction Conditions and the Nature of the Support of CoMo Catalysts. *J. Phys. Chem. B* **2006**, *110*, 2108–2115.

(18) Murakami, Y.; Miyauchi, Y.; Chiashi, S.; Maruyama, S. Direct Synthesis of High-Quality

Single-Walled Carbon Nanotubes on Silicon and Quartz Substrates. *Chem. Phys. Lett.* **2003**, *377*, 49–54.
(19) Li, X.; Tu, X.; Zaric, S.; Welsher, K.; Seo, W. S.; Zhao, W.; Dai, H. Selective Synthesis Combined with Chemical Separation of Single-Walled Carbon Nanotubes for Chirality Selection. *J. Am. Chem. Soc.* **2007**, *129*, 15770–15771.
(20) Miyauchi, Y.; Chiashi, S.; Murakami, Y.; Hayashida, Y.; Maruyama, S. Fluorescence Spectroscopy of Single-Walled Carbon Nanotubes Synthesized from Alcohol. *Chem. Phys. Lett.* **2004**, *387*, 198–203.
(21) Chiang, W.-H.; Sankaran, R. M. Linking Catalyst Composition to Chirality Distributions of as-Grown Single-Walled Carbon Nanotubes by Tuning NixFe1− X Nanoparticles. *Nat. Mater.* **2009**, *8*, 882–886.
(22) Xiang, R.; Einarsson, E.; Murakami, Y.; Shiomi, J.; Chiashi, S.; Tang, Z.; Maruyama, S. Diameter Modulation of Vertically Aligned Single-Walled Carbon Nanotubes. *ACS Nano* **2012**, *6*, 7472–7479.
(23) Ago, H.; Imamura, S.; Okazaki, T.; Saito, T.; Yumura, M.; Tsuji, M. CVD Growth of Single-Walled Carbon Nanotubes with Narrow Diameter Distribution over Fe/MgO Catalyst and Their Fluorescence Spectroscopy. *J. Phys. Chem. B* **2005**, *109*, 10035–10041.
(24) Wang, W.; Bai, X.; Xu, Z.; Liu, S.; Wang, E. Low Temperature Growth of Single-Walled Carbon Nanotubes: Small Diameters with Narrow Distribution. *Chem. Phys. Lett.* **2006**, *419*, 81–85.
(25) Wang, H.; Wang, B.; Quek, X.-Y.; Wei, L.; Zhao, J.; Li, L.-J.; Chan-Park, M. B.; Yang, Y.; Chen, Y. Selective Synthesis of (9, 8) Single Walled Carbon Nanotubes on Cobalt Incorporated TUD-1 Catalysts. *J. Am. Chem. Soc.* **2010**, *132*, 16747–16749.
(26) Li, N.; Wang, X.; Ren, F.; Haller, G. L.; Pfefferle, L. D. Diameter Tuning of Single-Walled Carbon Nanotubes with Reaction Temperature Using a Co Monometallic Catalyst. *J. Phys. Chem. C* **2009**, *113*, 10070–10078.
(27) Chen, Y.; Wei, L.; Wang, B.; Lim, S.; Ciuparu, D.; Zheng, M.; Chen, J.; Zoican, C.; Yang, Y.; Haller, G. L. Low-Defect, Purified, Narrowly (n, M)-Dispersed Single-Walled Carbon Nanotubes Grown from Cobalt-Incorporated MCM-41. *ACS Nano* **2007**, *1*, 327–336.
(28) He, M.; Chernov, A. I.; Fedotov, P. V.; Obraztsova, E. D.; Rikkinen, E.; Zhu, Z.; Sainio, J.; Jiang, H.; Nasibulin, A. G.; Kauppinen, E. I. Selective Growth of SWNTs on Partially Reduced Monometallic Cobalt Catalyst. *Chem. Commun.* **2011**, *47*, 1219–1221.
(29) Wang, H.; Wei, L.; Ren, F.; Wang, Q.; Pfefferle, L. D.; Haller, G. L.; Chen, Y. Chiral-Selective CoSO4/SiO2 Catalyst for (9, 8) Single-Walled Carbon Nanotube Growth. *ACS Nano* **2012**, *7*, 614–626.
(30) Wang, H.; Ren, F.; Liu, C.; Si, R.; Yu, D.; Pfefferle, L. D.; Haller, G. L.; Chen, Y. CoSO< Sub> 4/SiO< Sub> 2 Catalyst for Selective Synthesis of (9, 8) Single-Walled Carbon Nanotubes: Effect of Catalyst Calcination. *J. Catal.* **2013**, *300*, 91–101.
(31) Wang, H.; Goh, K.; Xue, R.; Yu, D.; Jiang, W.; Lau, R.; Chen, Y. Sulfur Doped Co/SiO2 Catalysts for Chirally Selective Synthesis of Single Walled Carbon Nanotubes. *Chem. Commun.* **2013**, *49*, 2031–2033.
(32) Fouquet, M.; Bayer, B.; Esconjauregui, S.; Blume, R.; Warner, J.; Hofmann, S.; Schlögl, R.; Thomsen, C.; Robertson, J. Highly Chiral-Selective Growth of Single-Walled Carbon Nanotubes with a Simple Monometallic Co Catalyst. *Phys. Rev. B* **2012**, *85*, 235411.
(33) Picher, M.; Anglaret, E.; Arenal, R.; Jourdain, V. Processes Controlling the Diameter Distribution of Single-Walled Carbon Nanotubes during Catalytic Chemical Vapor Deposition. *ACS Nano* **2011**, *5*, 2118–2125.
(34) He, M.; Jiang, H.; Liu, B.; Fedotov, P. V.; Chernov, A. I.; Obraztsova, E. D.; Cavalca, F.; Wagner, J. B.; Hansen, T. W.; Anoshkin, I. V. Chiral-Selective Growth of Single-Walled Carbon Nanotubes on Lattice-Mismatched Epitaxial Cobalt Nanoparticles. *Sci. Rep.* **2013**, *3*.
(35) Paillet, M.; Jourdain, V.; Poncharal, P.; Sauvajol, J.-L.; Zahab, A.; Meyer, J. C.; Roth, S.; Cordente, N.; Amiens, C.; Chaudret, B. Versatile Synthesis of Individual Single-Walled

Carbon Nanotubes from Nickel Nanoparticles for the Study of Their Physical Properties. *J. Phys. Chem. B* **2004**, *108*, 17112–17118.
(36) Li, Y.; Mann, D.; Rolandi, M.; Kim, W.; Ural, A.; Hung, S.; Javey, A.; Cao, J.; Wang, D.; Yenilmez, E. Preferential Growth of Semiconducting Single-Walled Carbon Nanotubes by a Plasma Enhanced CVD Method. *Nano Lett.* **2004**, *4*, 317–321.
(37) Thurakitseree, T.; Kramberger, C.; Zhao, P.; Aikawa, S.; Harish, S.; Chiashi, S.; Einarsson, E.; Maruyama, S. Diameter-Controlled and Nitrogen-Doped Vertically Aligned Single-Walled Carbon Nanotubes. *Carbon* **2012**, *50*, 2635–2640.
(38) Thurakitseree, T.; Kramberger, C.; Kumamoto, A.; Chiashi, S.; Einarsson, E.; Maruyama, S. Reversible Diameter Modulation of Single-Walled Carbon Nanotubes by Acetonitrile-Containing Feedstock. *ACS Nano* **2013**, *7*, 2205–2211.
(39) Paillet, M.; Meyer, J. C.; Michel, T.; Jourdain, V.; Poncharal, P.; Sauvajol, J.-L.; Cordente, N.; Amiens, C.; Chaudret, B.; Roth, S. Selective Growth of Large Chiral Angle Single-Walled Carbon Nanotubes. *Diam. Relat. Mater.* **2006**, *15*, 1019–1022.
(40) Wei, L.; Bai, S.; Peng, W.; Yuan, Y.; Si, R.; Goh, K.; Jiang, R.; Chen, Y. Narrow-Chirality Distributed Single-Walled Carbon Nanotube Synthesis by Remote Plasma Enhanced Ethanol Deposition on Cobalt Incorporated MCM-41 Catalyst. *Carbon* **2014**, *66*, 134–143.
(41) He, M.; Jiang, H.; Kauppinen, E. I.; Lehtonen, J. Diameter and Chiral Angle Distribution Dependencies on the Carbon Precursors in Surface-Grown Single-Walled Carbon Nanotubes. *Nanoscale* **2012**, *4*, 7394–7398.
(42) Wang, B.; Poa, C. P.; Wei, L.; Li, L.-J.; Yang, Y.; Chen, Y. (n, M) Selectivity of Single-Walled Carbon Nanotubes by Different Carbon Precursors on Co-Mo Catalysts. *J. Am. Chem. Soc.* **2007**, *129*, 9014–9019.
(43) Zhu, Z.; Jiang, H.; Susi, T.; Nasibulin, A. G.; Kauppinen, E. I. The Use of NH3 to Promote the Production of Large-Diameter Single-Walled Carbon Nanotubes with a Narrow (n, M) Distribution. *J. Am. Chem. Soc.* **2010**, *133*, 1224–1227.
(44) Pattinson, S. W.; Ranganathan, V.; Murakami, H. K.; Koziol, K. K.; Windle, A. H. Nitrogen-Induced Catalyst Restructuring for Epitaxial Growth of Multiwalled Carbon Nanotubes. *ACS Nano* **2012**, *6*, 7723–7730.
(45) Pattinson, S. W.; Rivas, R. D.; Stelmashenko, N.; Windle, A. H.; Ducati, C.; Stach, E. A.; Koziol, K. K. In-Situ Observation of the Effect of Nitrogen on Carbon Nanotube Synthesis. *Chem. Mater.* **2013**.
(46) Maultzsch, J.; Telg, H.; Reich, S.; Thomsen, C. Radial Breathing Mode of Single-Walled Carbon Nanotubes: Optical Transition Energies and Chiral-Index Assignment. *Phys. Rev. B* **2005**, *72*, 205438.
(47) Popov, V. N.; Henrard, L.; Lambin, P. Resonant Raman Intensity of the Radial Breathing Mode of Single-Walled Carbon Nanotubes within a Nonorthogonal Tight-Binding Model. *Nano Lett.* **2004**, *4*, 1795–1799.
(48) Popov, V. N.; Henrard, L.; Lambin, P. Electron-Phonon and Electron-Photon Interactions and Resonant Raman Scattering from the Radial-Breathing Mode of Single-Walled Carbon Nanotubes. *Phys. Rev. B* **2005**, *72*, 035436.
(49) Meyer, J. C.; Paillet, M.; Michel, T.; Moréac, A.; Neumann, A.; Duesberg, G. S.; Roth, S.; Sauvajol, J.-L. Raman Modes of Index-Identified Freestanding Single-Walled Carbon Nanotubes. *Phys. Rev. Lett.* **2005**, *95*, 217401.
(50) Pisana, S.; Cantoro, M.; Parvez, A.; Hofmann, S.; Ferrari, A.; Robertson, J. The Role of Precursor Gases on the Surface Restructuring of Catalyst Films during Carbon Nanotube Growth. *Phys. E Low-Dimens. Syst. Nanostructures* **2007**, *37*, 1–5.
(51) Chen, Y.; Ciuparu, D.; Lim, S.; Yang, Y.; Haller, G. L.; Pfefferle, L. Synthesis of Uniform Diameter Single-Wall Carbon Nanotubes in Co-MCM-41: Effects of the Catalyst Prereduction and Nanotube Growth Temperatures. *J. Catal.* **2004**, *225*, 453–465.
(52) Schüth, F.; Palkovits, R.; Schlögl, R.; Su, D. Ammonia as a Possible Element in an Energy Infrastructure: Catalysts for Ammonia Decomposition. *Energy Environ. Sci.* **2012**, *5*, 6278–

6289.
(53) Hansgen, D. A.; Vlachos, D. G.; Chen, J. G. Using First Principles to Predict Bimetallic Catalysts for the Ammonia Decomposition Reaction. *Nat. Chem.* **2010**, *2*, 484–489.
(54) Fukuda, Y.; Wayne Rabalais, J. Chemisorption of NO and NH< Sub> 3 on Cobalt: Studies by UPS, XPS, and Work-Function Measurements. *J. Electron Spectrosc. Relat. Phenom.* **1982**, *25*, 237–243.
(55) Cheng, H.; Huang, Y.; Wang, A.; Wang, X.; Zhang, T. Preparation of Cobalt Nitride from Co–Al Hydrotalcite and Its Application in Hydrazine Decomposition. *Top. Catal.* **2009**, *52*, 1535–1540.
(56) Parks, E.; Klots, T.; Winter, B.; Riley, S. Reactions of Cobalt Clusters with Water and Ammonia: Implications for Cluster Structure. *J. Chem. Phys.* **1993**, *99*, 5831.
(57) Kaghazchi, P.; Jacob, T.; Wang, H.; Chen, W.; Madey, T. E. First-Principles Studies on Adsorbate-Induced Faceting of Re (112 [over¯] 1). *Phys. Rev. B* **2009**, *79*, 132107.
(58) Esconjauregui, S.; Cepek, C.; Fouquet, M.; Bayer, B.; Gamalski, A.; Chen, B.; Xie, R.; Bhardwaj, S.; Ducati, C.; Hofmann, S. Plasma Stabilisation of Metallic Nanoparticles on Silicon for the Growth of Carbon Nanotubes. *J. Appl. Phys.* **2012**, *112*, 034303–034303.
(59) O'Byrne, J. P.; Li, Z.; Jones, S. L.; Fleming, P. G.; Larsson, J. A.; Morris, M. A.; Holmes, J. D. Nitrogen Chemical Vapour Deposition Synthesis of Carbon Nanotubes: **2011**, *12*, 2995–3001.
(60) Wang, Q.; Ng, M.-F.; Yang, S.-W.; Yang, Y.; Chen, Y. The Mechanism of Single-Walled Carbon Nanotube Growth and Chirality Selection Induced by Carbon Atom and Dimer Addition. *ACS Nano* **2010**, *4*, 939–946.
(61) Lu, C.; Liu, J. Controlling the Diameter of Carbon Nanotubes in Chemical Vapor Deposition Method by Carbon Feeding. *J. Phys. Chem. B* **2006**, *110*, 20254–20257.
(62) Maruyama, S.; Kojima, R.; Miyauchi, Y.; Chiashi, S.; Kohno, M. Low-Temperature Synthesis of High-Purity Single-Walled Carbon Nanotubes from Alcohol. *Chem. Phys. Lett.* **2002**, *360*, 229–234.
(63) Ding, L.; Tselev, A.; Wang, J.; Yuan, D.; Chu, H.; McNicholas, T. P.; Li, Y.; Liu, J. Selective Growth of Well-Aligned Semiconducting Single-Walled Carbon Nanotubes. *Nano Lett.* **2009**, *9*, 800–805.
(64) Hofmann, S.; Sharma, R.; Ducati, C.; Du, G.; Mattevi, C.; Cepek, C.; Cantoro, M.; Pisana, S.; Parvez, A.; Cervantes-Sodi, F. In Situ Observations of Catalyst Dynamics during Surface-Bound Carbon Nanotube Nucleation. *Nano Lett.* **2007**, *7*, 602–608.
(65) Wirth, C. T.; Bayer, B. C.; Gamalski, A. D.; Esconjauregui, S.; Weatherup, R. S.; Ducati, C.; Baehtz, C.; Robertson, J.; Hofmann, S. The Phase of Iron Catalyst Nanoparticles during Carbon Nanotube Growth. *Chem. Mater.* **2012**, *24*, 4633–4640.

Figures

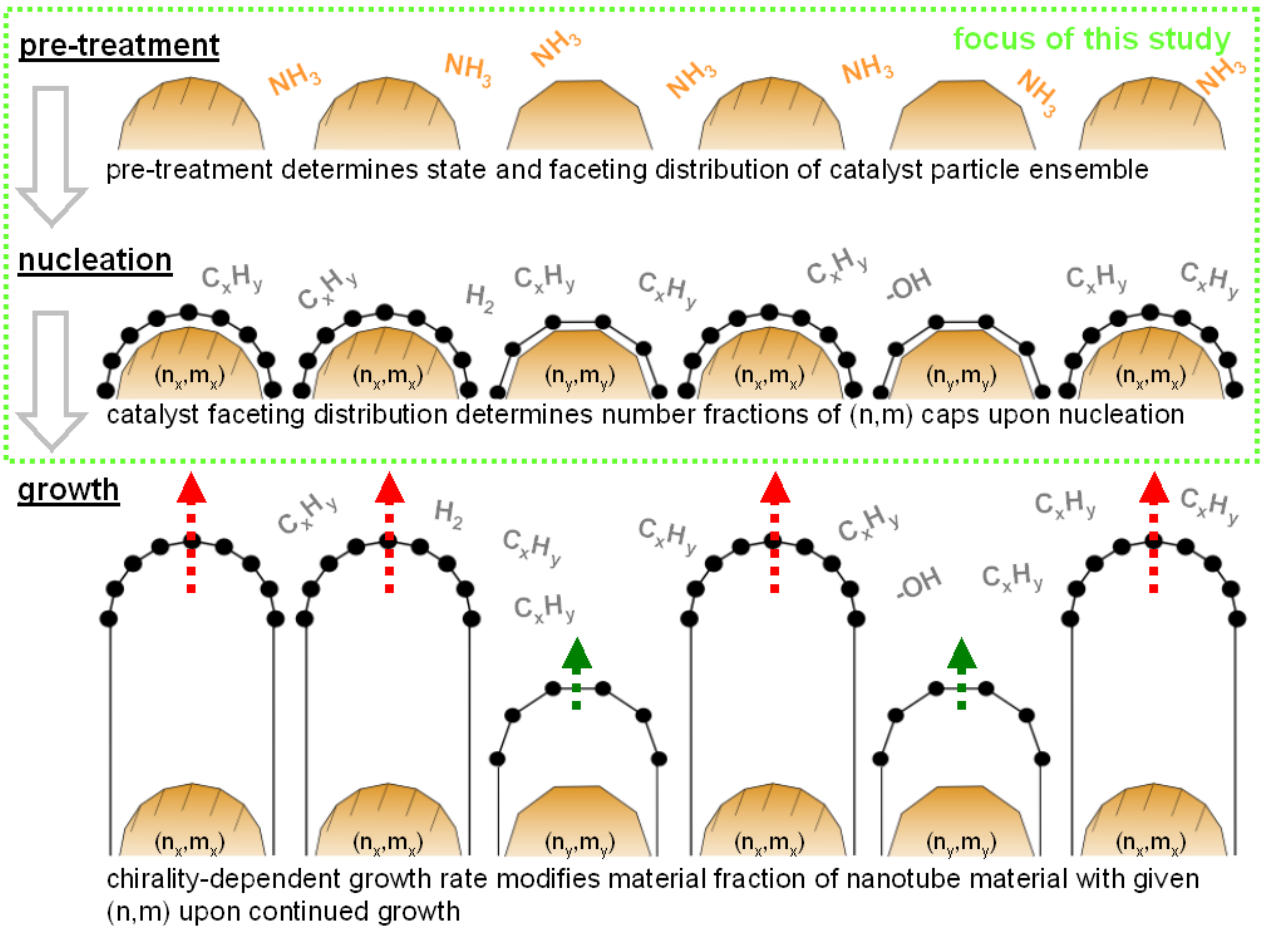

Figure 1: Schematic sketch of evolution of SWNT chiral abundance, as determined by the two discussed factors, exemplified by illustrations for two chiralities (n_x, m_x) and (n_y, m_y): (From top to bottom) Pre-treatment stage: Before introduction of the hydrocarbon precursor, pre-treatment conditions determine the state and faceting distribution of a catalyst particle ensemble. Then hydrocarbon is introduced: 1. Nucleation stage: First, at the point of SWNT nucleation, the relationship between the faceting/reconstruction of a given catalyst nanoparticle and a given nanotube cap leads to nucleation of a given (n, m) ensemble. This determines the initial number fraction of tubes with a particular chirality in a nanotube ensemble. 2. Continued growth stage: Secondly, during further growth of the nanotubes, chirality-dependent growth rates modify the material fraction of nanotube material with a particular (n, m) in a bulk sample of SWNTs. The focus of this study is the effect of pre-treatment on the chiral distribution, as highlighted with a green dashed frame in the sketch.

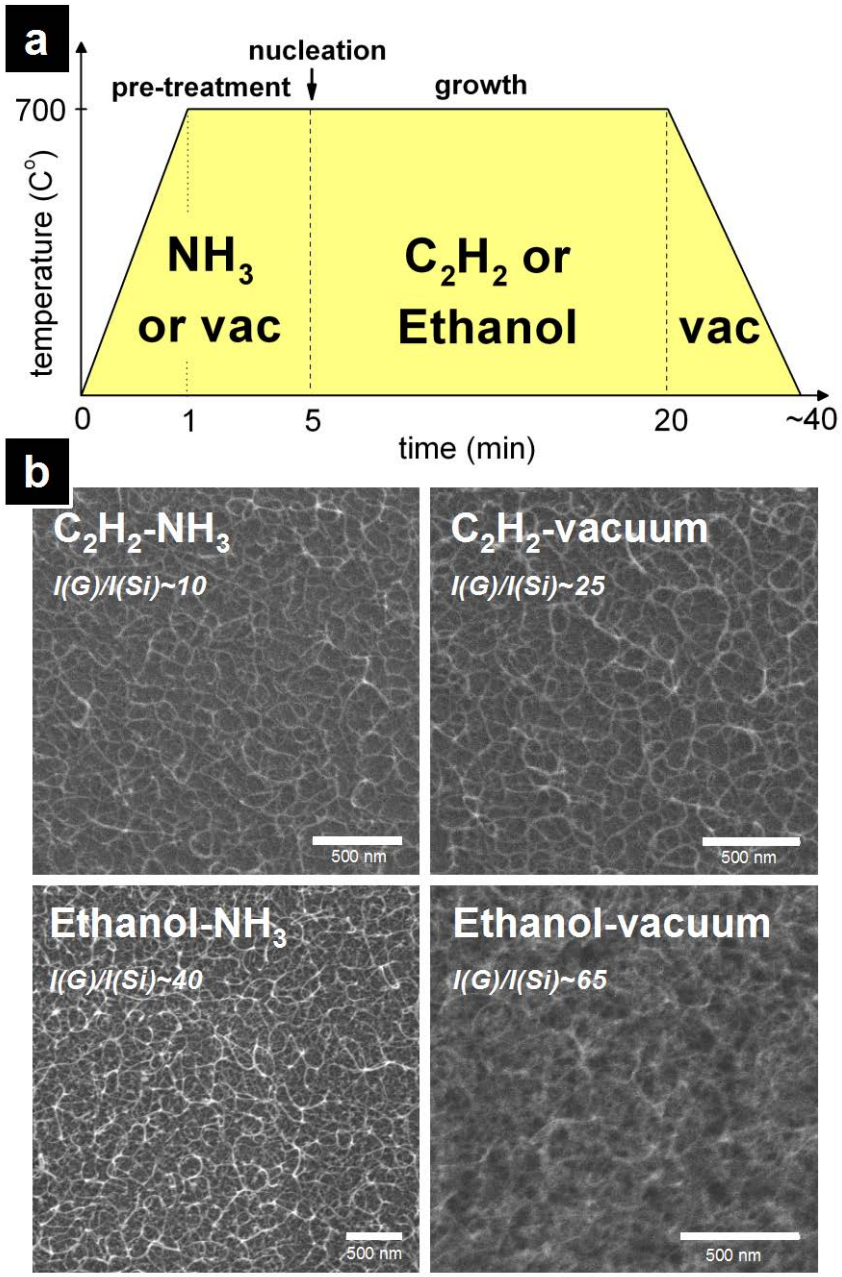

Figure 2: (a) Schematic process diagram for the two-step 700 ºC low pressure CVD growth, consisting of ramp up (1 min) and pre-treatment (4 min) in NH_3 or, for reference, vacuum, followed by introduction of pure hydrocarbon (C_2H_2 or Ethanol vapor, 15 min). The growth process is followed by a cool down in vacuum (times not to scale in sketch). (b) SEM images of the obtained nanotubes from the different hydrocarbon (C_2H_2 vs. Ethanol) and pre-treatment (NH_3 vs. vacuum) combinations. In the image labels a relative estimation for nanotube coverage for the various samples is given by calculating the ratio of the intensity G-peak region and the intensity of the Si-peak at 521 cm^{-1} (I(G)/I(Si)). An increase in I(G)/I(Si) indicates an increase in nanotube yield/coverage. For Ar pre-treatment the I(G)/I(Si) ratio is ~0.9, consistent with strongly reduced nanotube yield in SEM (not shown) for Ar-pretreated samples. (Note that the SEM image for C_2H_2/vacuum is from the same measurements as plotted in ref. [32])

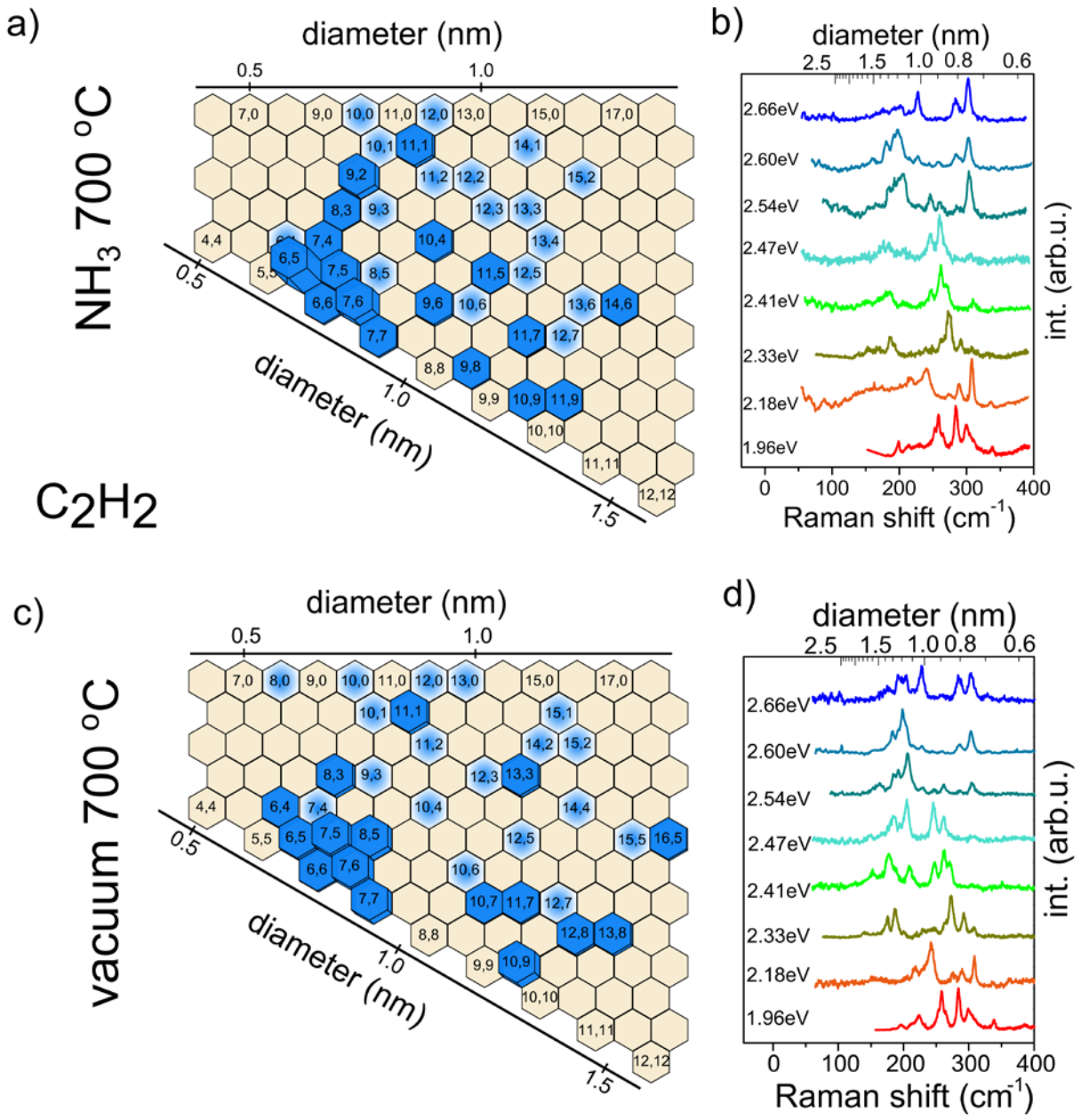

Figure 3: C_2H_2 growth – NH_3 versus vacuum pre-treatment: (a) Chiral map and (b) Raman spectra for the SWNTs grown by NH_3 pre-treatment followed by exposure to pure C_2H_2 at 700 ºC. (c) Chiral map and (d) Raman spectra for CVD by vacuum pre-treatment followed by C_2H_2 growth at 700 ºC. In the chiral maps the column height indicates the abundance (with abundances ≤1% in faded blue). Note that the data for (c) and (d) was taken from ref [32]. The raw data of the chiral maps is tabulated in the Supporting Information.

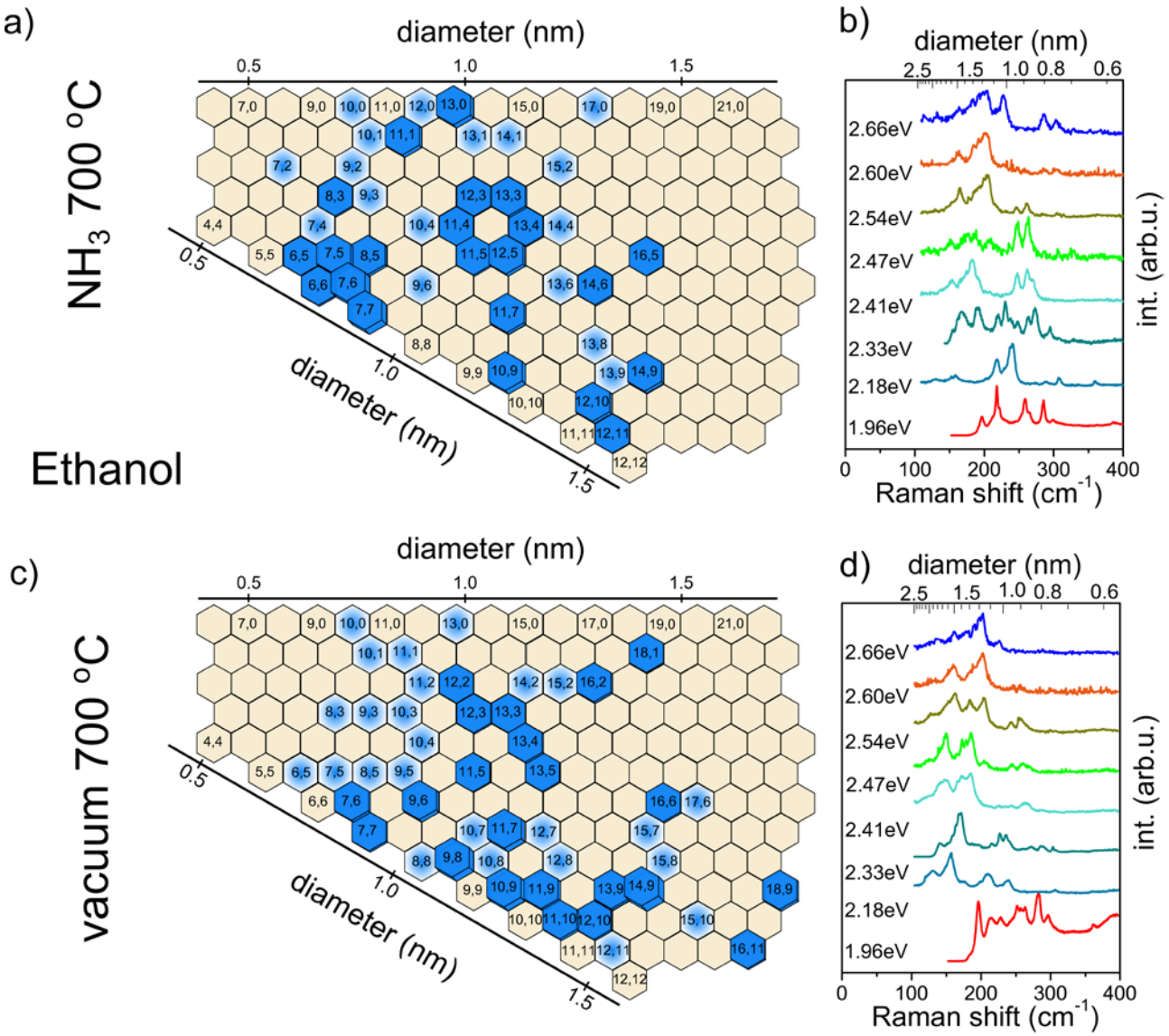

Figure 4: Ethanol growth – NH_3 versus vacuum pre-treatment: (a) Chiral map and (b) Raman spectra for the SWNTs grown by NH_3 pre-treatment followed by exposure to pure Ethanol at 700 ºC. (c) Chiral map and (d) Raman spectra for CVD by vacuum pre-treatment followed by Ethanol growth at 700 ºC. In the chiral maps the column height indicates the abundance (with abundances ≤1% in faded blue). The raw data of the chiral maps is tabulated in the Supporting Information.

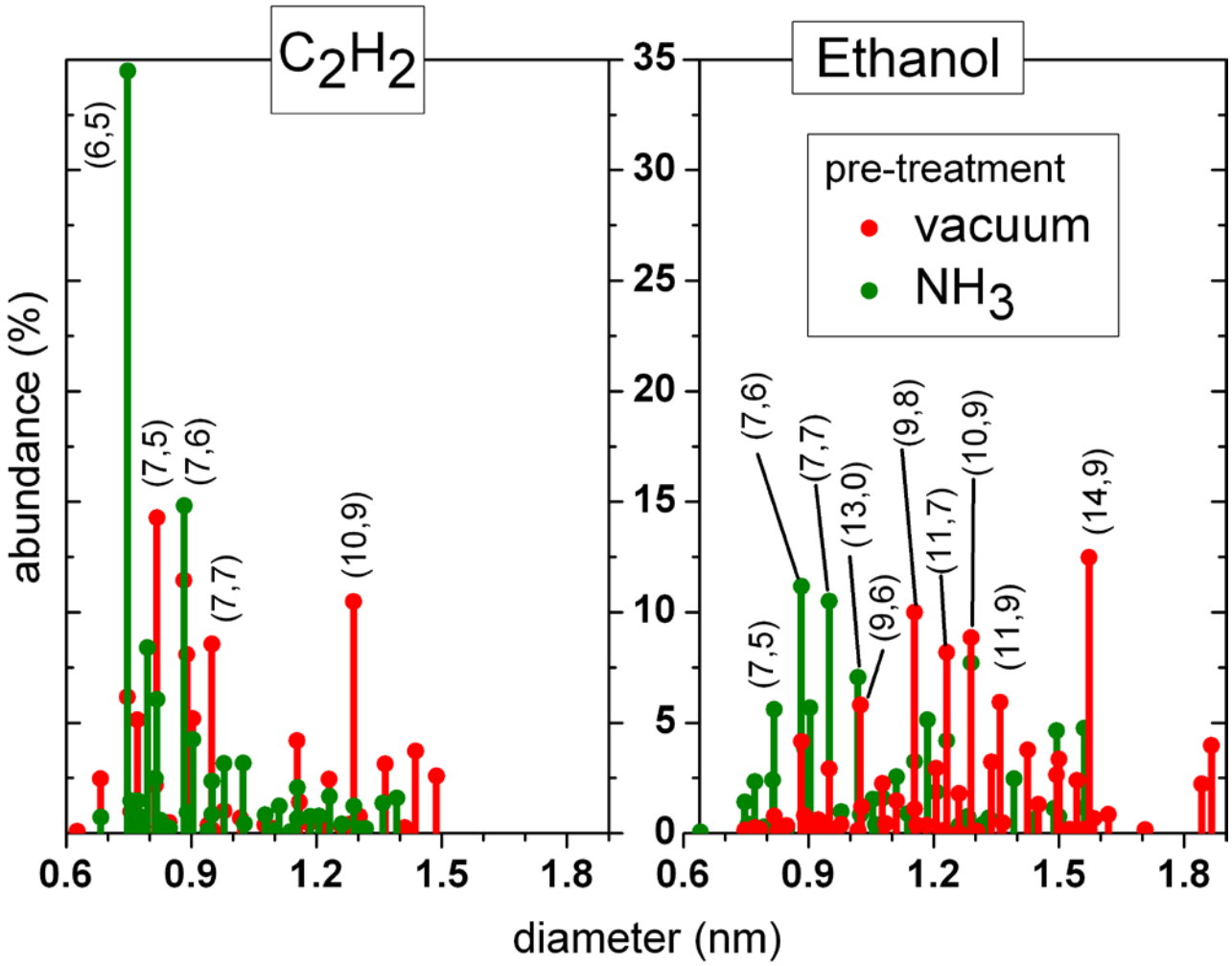

Figure 5: Estimated abundance as a function of tube diameter for all assigned (n, m) grown by C_2H_2 (left) and Ethanol (right) after pre-treatment in vacuum (red) or NH_3 (green), respectively.

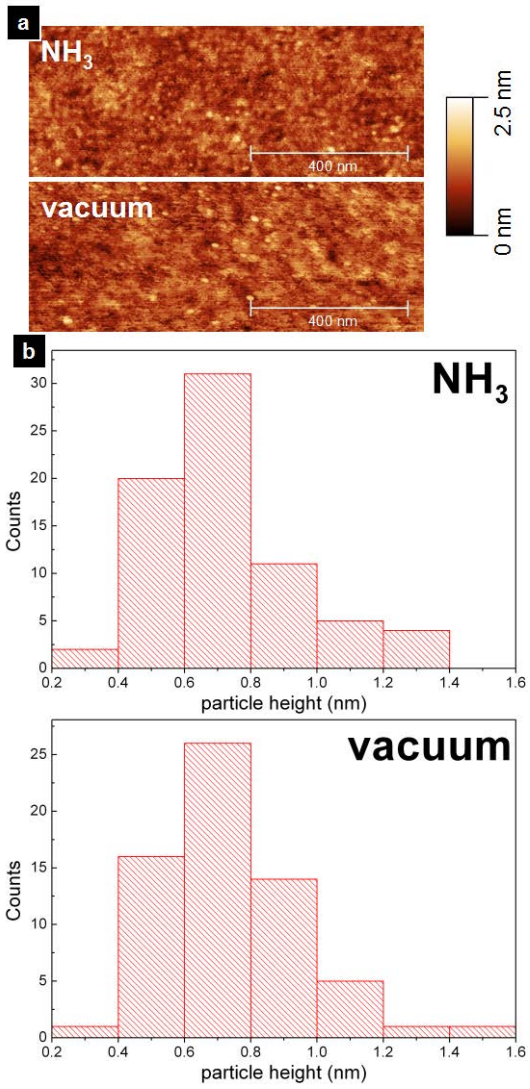

Figure 6: (a) AFM scans of samples that underwent pre-treatment in NH_3 or vacuum (i.e. no hydrocarbon exposure but immediate cooling in vacuum after pre-treatment), confirming nanoparticle formation during pre-treatment both NH_3 and vacuum pre-treatment (particle density estimated to ~1×10^{10} particles/cm^2). Similar AFM scans of samples that underwent pre-treatment in Ar (not shown) exhibit in comparison only very few nanoparticles, indicating that the strongly reduced nanotube yield from Ar pre-treatment is due to incomplete nanoparticle formation. (b) Histograms of particle heights derived from the AFM scans in (a). The particle heights were measured using AFM image processing software and manually identifying nanoparticles in 500 nm by 500 nm scans. We conclude from the height histograms that no significant differences between particle sizes are induced when comparing NH_3 and vacuum pre-treatment, indicating that the particle size distribution is mainly determined by the pre-treatment temperature under our low-pressure conditions.[32] (For further discussion of particle height/nanotube diameter relationships see the Supporting Information.)

Table of Contents (TOC) Figure